

Communication

Mapping the Spatial Distribution of Natural Gamma Dose Rates as a Baseline Study in the Province of Asti, Italy

Omar Del Monte ^{1,*}, Alessandro Paola ², Bertin Pérez ^{3,4,5,*}, Laszlo Sajo-Bohus ^{6,7}
and Daniel Palacios Fernández ⁵

¹ Vigili del Fuoco, Corpo Nazionale dei Vigili del Fuoco, 14100 Asti, Italy

² Vigili del Fuoco, Corpo Nazionale dei Vigili del Fuoco, 10095 Torino, Italy; alessandro.paola@vigilfuoco.it

³ Rad Elec Inc., Frederick, MD 21704, USA

⁴ Investigación, Desarrollo e Innovación, Anphysrad SAC, Lima 15074, Peru

⁵ Departamento de Ciencias, Pontificia Universidad Católica del Perú, Lima 15088, Peru; dpalaciosf@pucp.edu.pe

⁶ Laboratorio de Física Nuclear, Universidad Simón Bolívar, Caracas 1080 A, Venezuela; lsajo@usb.ve

⁷ Alba Regia Technical Faculty, Óbuda University, 8000 Szekesfehervar, Hungary

* Correspondence: omar.delmonte@vigilfuoco.it (O.D.M.); bertin.perez@pucp.edu.pe (B.P.)

Abstract: Natural background gamma rays and their effects on human health are essential components of both radiation protection and public concern. In the frame of these aspects, the mapping of the natural gamma dose rate values of the Province of Asti is given. The Asti Fire Brigade Command approved a project relating to the mapping of gamma radiation from the natural background in the territory of Asti. The project engaged both the Nuclear, Biological, Chemical, and Radiological (NBCR) and Topography Applied to Rescue (TAS) components of the Asti Command. Skilled personnel, comprising level 1 TAS operators for data collection and level 2 TAS operators for cartographic analysis, were deployed across the six working days. The methodology involved the use of two digital handheld radiation G-M detectors, in conjunction with a portable GPS unit, including the *Global Mapper* software. One of the significant findings of this study is the observation that the natural gamma dose rate levels were 201.25% higher in the streets of the city center compared to other areas, predominantly because the building materials in these locations contain a higher amount of natural radionuclides. The results indicated that the level of natural gamma dose rates in the studied region is close to the global average value.

Keywords: radioactive pollutant; dose rate; environmental dosimetry; map; Asti; Italy



Citation: Del Monte, O.; Paola, A.; Pérez, B.; Sajo-Bohus, L.; Palacios Fernández, D. Mapping the Spatial Distribution of Natural Gamma Dose Rates as a Baseline Study in the Province of Asti, Italy. *Pollutants* **2024**, *4*, 174–186. <https://doi.org/10.3390/pollutants4020011>

Academic Editor: Ilaria Guagliardi

Received: 15 November 2023

Revised: 8 February 2024

Accepted: 26 March 2024

Published: 2 April 2024



Copyright: © 2024 by the authors. Licensee MDPI, Basel, Switzerland. This article is an open access article distributed under the terms and conditions of the Creative Commons Attribution (CC BY) license (<https://creativecommons.org/licenses/by/4.0/>).

1. Introduction

Natural background radiation is a pervasive aspect of our environment, arising from sources like the Earth's crust, cosmic rays, and atmospheric radioactive isotopes. This radiation is crucial for health studies, radiation protection, and risk assessment [1]. It serves as a baseline exposure that constantly affects human health, aiding in understanding the risks associated with additional radiation sources and establishing safety standards. This knowledge helps in formulating guidelines and setting protection measures for various occupational and environmental settings. Studies have explored the potential health effects linked to high natural background radiation areas, emphasizing the need for comprehensive epidemiological studies [2].

Understanding the contribution of natural background radiation is important in assessing the overall radiological risk for the population within different geographical regions. This knowledge is vital for resource allocation and priority setting in radiation protection. Educating the public about the relative risks of various radiation sources is essential to ensure informed decision making, especially in regions with high variability in Naturally Occurring Radioactive Material (NORM) [3] and other potential exposure instances [4].

Although natural radiation exposure generally poses low health risks, it contributes to setting safety standards and guidelines for radiation use in various applications. Additionally, there is a need for a regulatory framework to mitigate radiological risks. It is essential to account for potential accidents, involving radioactive substances in various sectors, including medical, civil, and military fields, and the potential risks associated with nuclear energy use and nuclear waste management [5–9].

The spatial distribution of natural radioactivity in various countries is a topic of interest in environmental science and radiation protection. Natural radioactivity primarily arises from the presence of primordial radioactive elements such as ^{238}U , ^{232}Th , and ^{40}K in the Earth's crust [10–13]. The distribution of these elements can vary significantly from one region to another and depends on the geological composition of a specific region. Certain rocks, soils, and minerals contain these radioactive elements [14–18]. Areas with higher concentrations of these elements tend to exhibit higher natural background radiation levels. Radionuclides from the ^{238}U and ^{232}Th decay series in the Earth's crust undergo beta or alpha decay and may leave the residual nucleus in an excited state. In such instances, the nucleus can emit one or more gamma rays to transition to the ground state. These gamma rays contribute to background radiation. For instance, gamma rays emitted by radon and its decay products, along with those from ^{238}U and ^{232}Th decay chains, contribute significantly to natural background radiation. The actual exposure to gamma rays can vary widely based on geographical location. Some regions have higher natural background radiation due to geological factors, while others have lower levels [19]. Certain human activities can also influence local radiation levels. Mining, construction materials sourced from specific geological formations, or areas with higher levels of radioactive minerals can elevate background radiation. Radiation exposure is measured in units called sieverts (Sv). The millisievert (mSv) is a smaller unit used to express doses from natural sources, medical procedures, or occupational exposures. The annual average dose from natural background radiation varies globally, but it typically falls within the range of 1 to 10 mSv per year. Therefore, populations could be exposed to an annual effective dose reaching a maximum of 10 mSv per year, this maximum is equivalent to a dose rate of $1.14 \mu\text{Sv}\cdot\text{h}^{-1}$. Assuming an annual effective dose of let us say 2.4 mSv per year for a person life time of 70 years is around 168 mSv [20]. The latter is only an estimate since measurements have revealed a larger interval of values, i.e., 70–800 mSv, which is a justification supporting the present study [21].

Environmental radiation studies are carried out by monitors, nuclear spectroscopy, radon measurements, and geological surveys to quantify the levels of natural radiation levels [19,22–25]. The information obtained from these studies often is reported as maps; the values of the radiation levels and dose gradients are crucial for assessing potential health risks, establishing radiation protection guidelines, and developing strategies for managing areas with elevated natural radioactivity [26–28].

The European Union has funded projects such as the European Radiological Data Exchange Platform (EURDEP) to collect and share data on environmental radioactivity. This collaborative effort helps in understanding the spatial distribution of natural radioactivity on a continental scale [29]. Further information can be found at the site of the EURDEP system (<https://remon.jrc.ec.europa.eu/About/Rad-Data-Exchange> (accessed on 27 March 2024)). A collection of maps were conveniently produced as 'The European Atlas of Natural Radiation', intended to have a useful reference material (<https://remap.jrc.ec.europa.eu/Atlas.aspx> (accessed on 27 March 2024)).

Around the world, several programs have been conducted in the past to assess and map the spatial distribution of natural radioactivity surrounding the human habitat. These studies often included the measurement of radiation levels in soil, water, and air, as well as the examination of specific geological formations. Regions rich in monazite minerals that contain thorium have been inspected, and elevated levels of natural radioactivity sands were reported in Brazil [30], Egypt [31], India [32,33], Iran [34], Malaysia [35], Bangladesh [36], China [37], and others [38,39]. Radiological aspects related to the pri-

mordial radioactive families ^{238}U , ^{232}Th , ^{226}Ra , and ^{40}K , combined with the distribution characteristics of presumably contaminating elements, were seldom simultaneously investigated in rare-earth element (REE)-processing activities [37]. The U.S. Environmental Protection Agency (EPA, <https://www.epa.gov> (accessed on 27 March 2024)) regularly monitors natural radioactivity levels across the country including radionuclides in soil and water.

In our case, a comprehensive mapping study was conducted in the city of Asti to understand natural gamma dose rate levels in different areas, aiming to predict absorbed doses in case of a radiological emergency and to assess the presence of radioactive materials in different scenarios, including potential accidents, waste management, and the possibility of terrorist actions involving radioactive substances. This type of radiological emergency could refer to an incident involving the unexpected release or dispersion of radioactive materials on a scale that could have effects beyond local borders, that is at a regional or even global level. This study serves as a baseline. By conducting a comprehensive mapping of natural gamma dose rate levels in different areas of Asti, it establishes an initial reference for normal radiation levels in the region. This information is crucial for comparing and assessing any sudden changes or increases in radiation levels that may occur in the future. The study focused on provincial areas due to the responsibilities of the fire department in emergencies or accidents, and this initiative stemmed from the establishment of nuclear waste storage depots in the Municipality of Bosco Marengo, near our territorial borders. This necessitated mapping due to the anticipated transit of such materials. In addition, the varying intensity of ionizing radiation in the city center may be attributed to the presence of more radioactive building materials than others. The radioactivity of buildings can vary due to certain materials that may contain a higher concentration of natural radioactive elements, such as ^{238}U , ^{232}Th , and ^{226}Ra [40–43].

This pioneering effort represents the first comprehensive environmental assessment of the existing exposure situation in the city of Asti of its kind at a national level. Despite the significance of measuring radon concentration, which is abundant in Asti's wine cellars due to the tuff construction, the study focused on gamma-emitting natural radionuclides as a primary concern.

A radiological map of the mentioned region is important in the context of monitoring and managing radiation levels; it is required for assessing and ensuring the safety of the public, in order to take necessary measures in the event of a radiological emergency. There is a consensus that having a pre-existing radiological map in an emergency is invaluable. On the other hand, the collected information is vital for conservation efforts and sustainable environmental management. Radiological maps are essential for ensuring compliance with regulatory standards and guidelines related to radiation exposure. They provide a basis for setting limits, conducting regular assessments, and implementing corrective actions to meet established safety standards. In a global context, radiological maps contribute to international cooperation on nuclear safety and environmental protection. Sharing accurate and up-to-date information is essential for managing the impacts of radiation in a given region or country.

2. Materials and Methods

The mapping of Asti's territory was strategically organized into six zones for the ease of assessment, allowing comprehensive coverage of the region. The utilization of specialized equipment, including dosimeters and specific vehicles for traversing the areas, facilitated the collection of essential data for the project. Additionally, cartographic representations of the collected data will be made available to the relevant officials for further analysis and emergency response strategies.

This unique project not only contributes to setting safety standards, but also equips first responders with essential data to calculate potential absorbed doses in case of an incident. The gathered information will support the accurate zoning of affected areas, aiding in efficient emergency response operations.

2.1. Site Selection

The Province of Asti, located between 44°32'00" and 45°08'00" north latitude and 7°52'00" and 8°31'00" east longitude, is situated in the central-southern part of Piedmont and is one of the smallest Piedmontese provinces, covering a territorial extension of 1510.78 km², equal to 5.95% of the entire regional area.

The Province is predominantly hilly, with the maximum altitude reaching 845 m above sea level and the minimum hovering around 100 m. Among the 118 municipalities comprising the province, 18 are situated in the lowland area, 88 in the hilly region, and 12 in the mountainous area.

The geographical components shaping the territory of the Province of Asti encompass a segment of the Tanaro Valley, which encompasses the majority of the flat surface within the province. This is followed by the western portion of the Lower Monferrato, a part of Alto Monferrato, and a section of the Langhe in the far southern area. The southern part is primarily characterized by a foothill and mountainous landscape, merging into the Apennine border regions between Piedmont and Liguria.

The province's terrain is predominantly composed of sedimentary rocks formed through marine deposition, occasionally interrupted by terrestrial formations. These geological structures span from the Eocene–Cretaceous to the Quaternary periods. In the Lower Monferrato region, the oldest formations of distinct Apennine affinity emerge due to intense tectonic deformations. Over these formations, younger layers up to the Upper Miocene are deposited, primarily composed of alternating sandstone and marl; the first is a sedimentary rock composed of sand-sized mineral particles, primarily quartz, feldspar, and other minerals associated with the presence of ²³⁸U, ²³²Th, and their decay products. Marl is another type of sedimentary rock that contains a variable mixture of clay and carbonate minerals with low radioactive content of ²³⁸U, ²³²Th, and decay products.

Similar lithological formations can be found in Alto Monferrato and the Langhe, but the structural arrangement is less disturbed, with Miocene formations consistently dipping towards the north.

The area between Langhe and Basso Monferrato is often referred to as the 'Pliocene Basin of Asti', where sand and clay with a rich deposit of marine fossils are present.

The western region of the Province is characterized by significant continental deposits of the Villafranchian age, comprising sandy soils and clayey alternations containing plant fossils such as trunks, leaves, and remnants of large terrestrial mammals.

2.2. Measurements and Dosimetry

In early 2021, the Provincial Fire Command of Asti initiated discussions within the Provincial NBCR center regarding mapping the natural environment. These surveys serve a dual purpose: establishing reference values for potential interventions and providing training for NBCR staff on tools (RADOS RDS-30, FH40 G) and TAS1/TAS2 staff on GPS and IT media, respectively. Collaboration between NBCR and the provincial TAS core facilitated geo-locating each measurement and sharing information for operational use. All measurements were digitally recorded on Google Earth for easy access. The project was divided into Provincial Mapping sessions, both within and outside the Municipality of Asti.

The survey characterization plan, following the procedure outlined in IAEA TEC DOC 1017 [44], initiated with site investigation and gathering information on the environmental background. Preceding the sampling, a reconnaissance of the area of interest was conducted to gather all available information pertinent to the site's history. The chosen characterization plan aimed for expediency, focusing on a procedure primarily centered on identifying areas of heightened radioactivity, or 'hot spots', in terms of external radiation from the soil. Ensuring accuracy in operator pathways during measurements, as well as the correct geographic identification and repeatability of the most radiometrically significant points necessitated the utilization of the Geographic Information System (GIS). Subsequently, the measurements were manipulated using *ArcGIS Online*.

Radiometric Mapping

The selection of sampling points followed a strategy focused on identifying radioactivity 'hot spots'. This involved systematic monitoring of gamma dose rates emitted by the soil, starting with a verification of the background value in an uncontaminated area for comparative purposes (background value detected of approximately $0.120 \mu\text{Sv} \cdot \text{h}^{-1}$).

To facilitate organized monitoring, the monitored area was divided into five zones: northwest (NW), northeast (NE), southwest (SW), southeast (SE), and the historic center of Asti (CE). Additionally, highways were monitored separately, as depicted in Figure 1. NBCR operators from the Asti Command employed the FH40 G electronic dosimetric instrumentation provided by the NBCR Unit to map the territory. The Thermo Scientific FH 40 G is a wide-range digital Geiger counter suitable for almost all measurement tasks related to radiation protection. It possesses a sensitivity of $>30 \text{ keV}$ and a dose range of $10 \mu\text{R}$ – 1000 R . This device is also certified for use by German fire brigades and has been tested by Physikalisch-Technische Bundesanstalt (PTB) (<https://www.ptb.de/cms/>) (accessed on 27 March 2024). This device is also designed to conform to the energy response behavior required for the new SI units of the ambient dose equivalent and ambient dose equivalent rate, following ICRU 39 standards [45].

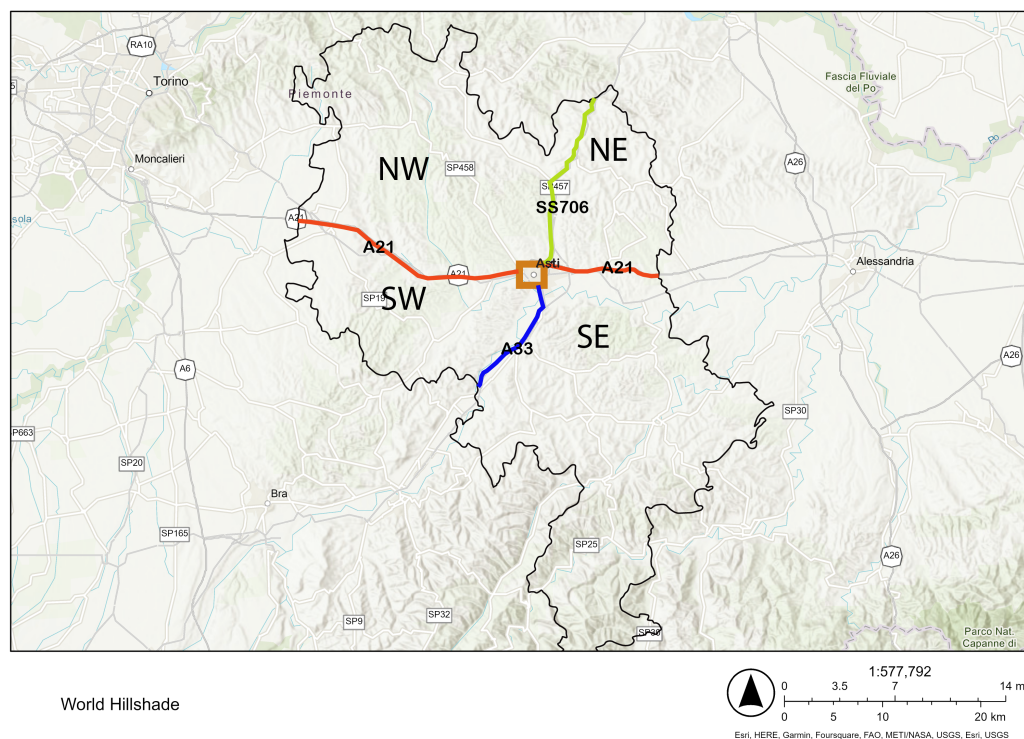


Figure 1. Map of the Province of Asti (black line) showing the historic center as an orange rectangle and the northwest, southwest, southeast, and northeast subdivisions, along with the important highways A21 (red line), A33 (blue line), and SS706 (green line) where the assessments were conducted.

Operations in the historic center (at the Municipality level) were conducted on foot during six days, each lasting nine hours (first survey). However, due to the extensive provincial territory outside the Municipality, another survey was carried out using vehicles for an additional six days (second survey). Operators would stop approximately every 200 m, disembarking to conduct measurements. Within and outside the Municipality, the dose rates were measured about 50 cm above the ground using gamma counting with the FHZ 512 scintillator connected to the FH 40 G radiometer. In addition, both surveys were conducted in March.

3. Results and Discussion

The values of the natural gamma dose rates obtained by the FH 40 G device in the first survey ranged from 0.04 to 0.42 $\mu\text{Sv}\cdot\text{h}^{-1}$ and in the second survey from 0.03 to 0.23 $\mu\text{Sv}\cdot\text{h}^{-1}$.

Both surveys are statistically described in Tables 1 and 2.

Table 1. Summary statistic of natural gamma dose rates ($\mu\text{Sv}\cdot\text{h}^{-1}$) of the first survey.

	Meas.	Min	Max	Mean	Median	Mode	STD	Variance	Range	Skewness	Kurtosis
A21	34	0.06	0.22	0.0906	0.0849	0.06	0.0365	0.0013	0.16	2.1848	5.2456
A33	16	0.08	0.16	0.1162	0.11	0.11	0.0171	0.0003	0.08	0.5822	2.8249
SS706	21	0.11	0.13	0.1205	0.12	0.12	0.0067	4.47×10^{-5}	0.02	-0.0519	-0.4978
CE	49	0.1	0.42	0.2161	0.19	0.18	0.0803	0.0064	0.319	1.112	0.7158
NE	87	0.06	0.13	0.1055	0.10	0.09	0.0165	0.0002	0.07	0.1827	-0.8029
NW	52	0.04	0.15	0.1133	0.13	0.14	0.0385	0.0015	0.109	-1.1742	-0.3672
SE	55	0.08	0.16	0.1187	0.11	0.11	0.0179	0.0003	0.08	0.3571	0.2118
SW	58	0.05	0.17	0.1241	0.12	0.12	0.0256	0.0007	0.12	-0.4804	0.7628

Table 2. Summary statistic of natural gamma dose rates ($\mu\text{Sv}\cdot\text{h}^{-1}$) of the second survey.

	Meas.	Min	Max	Mean	Median	Mode	STD	Variance	Range	Skewness	Kurtosis
NE	100	0.07	0.14	0.1125	0.12	0.12	0.0177	0.0003	0.07	-0.5242	-0.6049
NW	120	0.04	0.23	0.104	0.10	0.10	0.0282	0.0008	0.19	1.0239	3.0236
SE	226	0.03	0.19	0.1021	0.11	0.11	0.0229	0.0005	0.16	-0.1807	1.0869
SW	170	0.06	0.15	0.1025	0.10	0.11	0.0164	0.0003	0.09	-0.2098	0.1268

Upon analyzing two distinct surveys of data regarding natural gamma dose rates, significant differences and similarities emerged in their statistical characteristics.

In the first survey (Table 1), comparing the minimum and maximum values across these locations revealed that the NW exhibits the lowest minimum dose rate of 0.04 $\mu\text{Sv}\cdot\text{h}^{-1}$, while the CE shows the highest maximum dose rate of 0.42 $\mu\text{Sv}\cdot\text{h}^{-1}$. The mean values offer a clearer picture of the average dose rates in each location, showing considerable variation. For instance, the CE demonstrates the highest mean dose rate of 0.2161 $\mu\text{Sv}\cdot\text{h}^{-1}$, while A21 exhibits the lowest mean of 0.0906 $\mu\text{Sv}\cdot\text{h}^{-1}$. However, the median values in some locations, like A21 and the NE, are notably lower than their respective means, indicating potential skewness towards lower values in these areas. Examining the variability using the standard deviation (STD), it is apparent that the measurements in the CE had the highest variability (0.0803 $\mu\text{Sv}\cdot\text{h}^{-1}$), suggesting a wider spread of data points around the mean compared to other locations. This is reinforced by the CE also having the highest variance (0.0064). The skewness and kurtosis values provide insight into the distribution shape and tail behavior. Positive skewness, seen in A21 and the NW, indicates a tail towards higher values, while negative skewness, evident in the NE and SS706, suggests a tail towards lower values. Additionally, kurtosis values above or below zero highlight the presence of heavier or lighter tails, respectively, concerning a normal distribution. Overall, these statistics collectively depict the diverse nature of gamma dose rates across the surveyed locations, reflecting substantial variability and distribution patterns that warrant further investigation and analysis.

In the second survey (Table 2), the SE showed the lowest minimum dose rate of 0.03 $\mu\text{Sv}\cdot\text{h}^{-1}$, while the NW exhibited the highest maximum dose rate of 0.23 $\mu\text{Sv}\cdot\text{h}^{-1}$. This means that when comparing the first survey with the second survey, the highest values were found within the CE, and this is also evident in the mean report of both surveys. The standard deviation (STD) values, indicative of data dispersion around the mean, ranged from 0.0164 to 0.0282, suggesting varying levels of spread in the measured gamma dose rates within the regions. The variance values were relatively low, ranging from 0.0003 to 0.0008, indicating a relatively clustered dataset. Moreover, the skewness and kurtosis values

provide insights into the shape of the distribution. Negative skewness values for the NE, SE, and SW regions (-0.5242 , -0.1807 , and -0.2098 , respectively) suggest a slight left-leaning asymmetry, implying a heavier tail on the left side of the distribution. The NW region, however, displayed positive skewness (1.0239), indicating a right-leaning asymmetry and a heavier tail on the right side. The kurtosis values, measuring the tailedness of the distribution, were negative for the NE, SE, and SW regions (-0.6049 , 1.0869 , and 0.1268 , respectively), suggesting relatively flatter distributions compared to a normal distribution. Notably, the NW region exhibited higher positive kurtosis (3.0236), indicating a more peaked and heavy-tailed distribution.

The behaviors of both surveys are depicted in Figure 2.

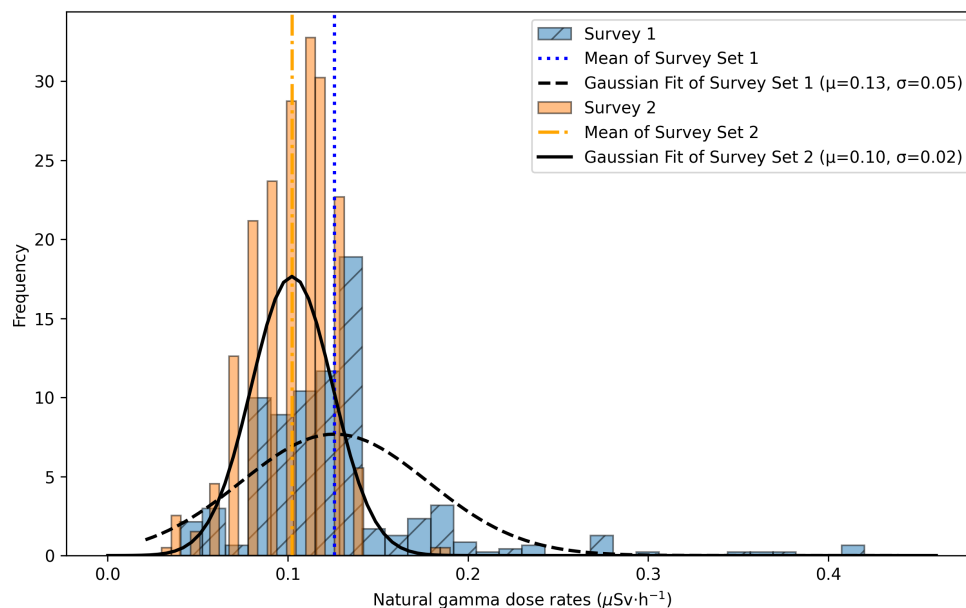


Figure 2. Bar histogram displaying the distribution of the measurements for both surveys.

Moreover, a notable difference arose in the results of the t-test conducted on both survey datasets. The results indicate a significant difference between both datasets, evident from a remarkably low p -value (3.7×10^{-15}). Figure 2 graphically illustrates that survey 1 had a higher average value and demonstrated greater variability around its mean. This reinforces the existence of anomalous dose rate values within survey 1, potentially indicating its association with the CE region, while ‘normal’ values are as expected and published by [46].

This distinction is clearly evident in the graphical representations displayed in Figures 3 and 4.

In Figures 3 and 4, the delineated area marked by the black line corresponds to the Province of Asti. A noteworthy observation is that the outliers identified in Figure 4, especially high values, fall within the range of values obtained in Figure 3. This suggests that the background radiation dose outside the boundaries of the Municipality of Asti is relatively low, comparing with overall results.

Moreover, high outlier values in Figure 3 evidence elevated background radiation levels concerning the entire studied area. These outliers, depicted by red dots in Figure 3, may be attributed to either natural geological variations or potential anthropogenic influences. The exploration of these outliers is crucial for understanding the nuances of the background radiation landscape within the Province of Asti. In Figure 5, a heat map is presented, offering a visual representation of the presence of high outlier values within the Municipality of Asti, with a particular emphasis on the historical center of the Municipality.

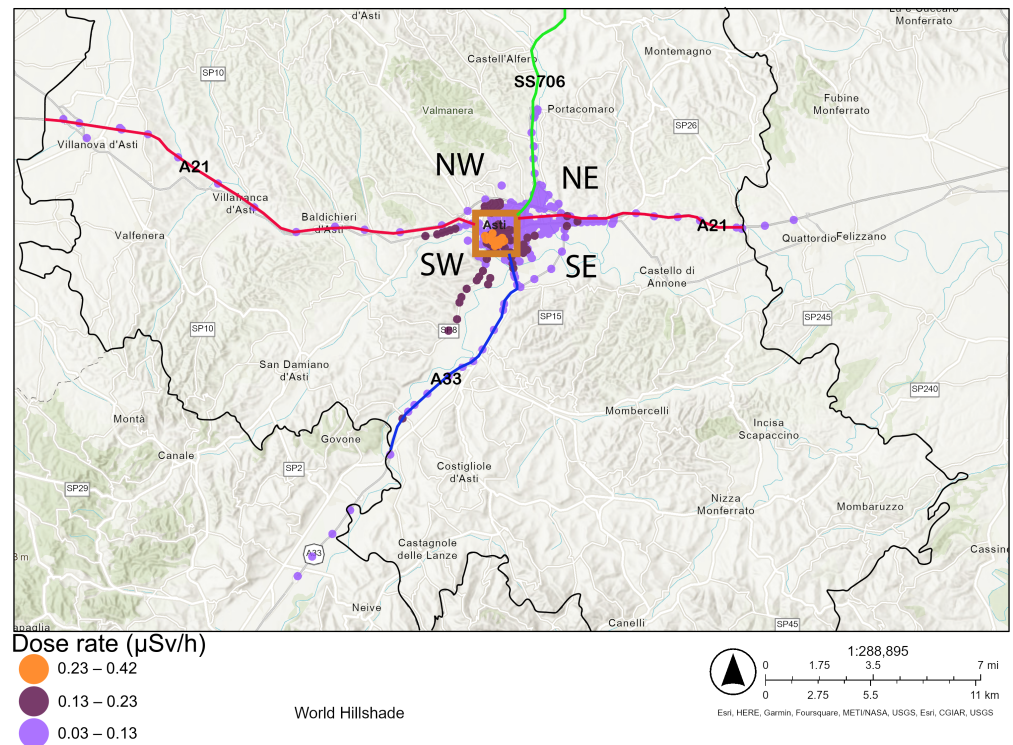


Figure 3. Dose rate map of the Municipality of Asti (first survey) ranging from 0.04 to 0.42 $\mu\text{Sv}\cdot\text{h}^{-1}$. Delimitation of the Province of Asti (depicted by the black line) and the historic center marked within an orange rectangle. Additionally, the northwest, southwest, southeast, and northeast subdivisions are indicated, along with the prominent highways: A21 (red line), A33 (blue line), and SS7066 (green line).

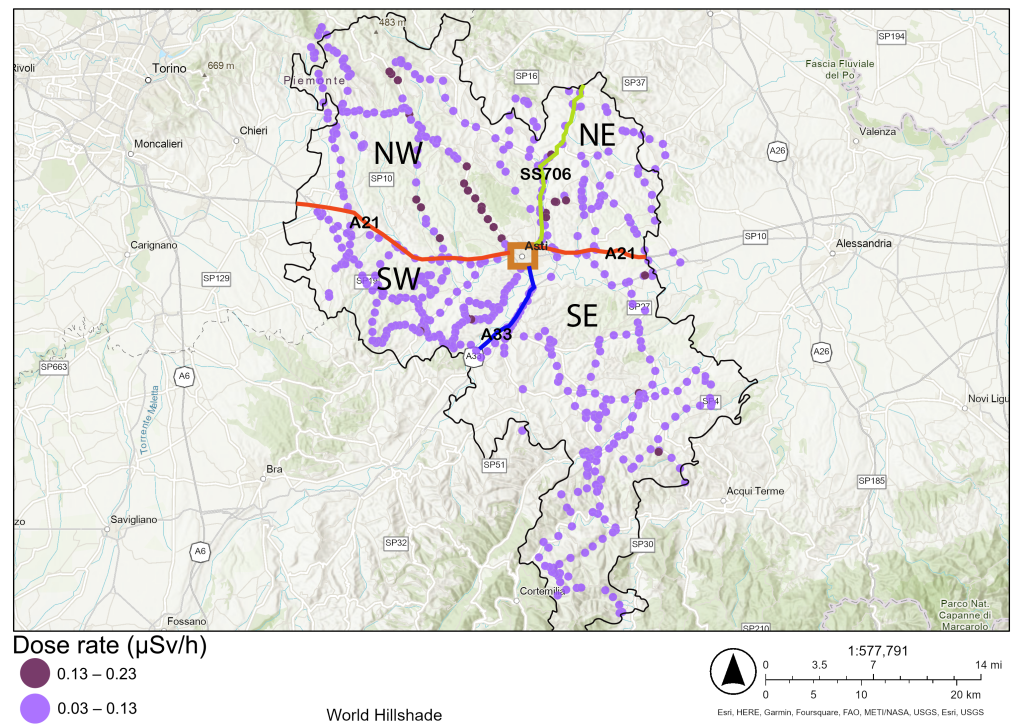


Figure 4. Dose rate map of the outskirts of the Municipality of Asti (second survey); ranges from 0.03 to 0.23 $\mu\text{Sv}\cdot\text{h}^{-1}$. Delimitation of the Province of Asti (depicted by the black line) and the historic center marked within an orange rectangle. Additionally, the northwest, southwest, southeast, and northeast subdivisions are indicated, along with the prominent highways: A21 (red line), A33 (blue line), and SS7066 (green line).

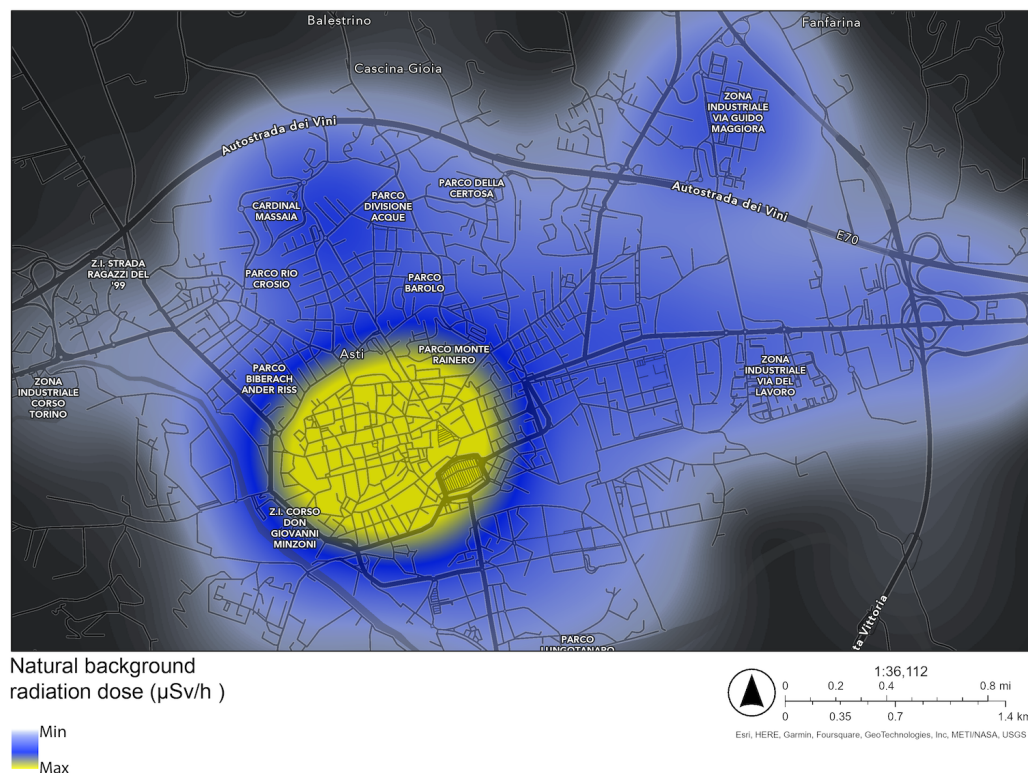


Figure 5. Natural gamma dose rate map of the Municipality of Asti, focused on the historic center of the area.

This localized concentration of high radiation, vividly depicted by the yellow zone in Figure 5, can be attributed to the prevalence of igneous rocks, specifically the pórfido and lucerna rocks (as reported in [47]), abundant in the region. Porphyry is a type of igneous rock characterized by large crystals (phenocrysts) embedded in a fine-grained matrix or ground mass. The radioactive content of porphyry can depend on the specific minerals present and their composition. For example, minerals like zircon, apatite, and certain feldspars can contain higher concentrations of uranium and thorium. The presence of these rocks in the materials used for road pavement within the historic center of the Municipality stands as a probable source contributing to the escalated radiation levels observed, as shown in Figure 5. The specific mechanisms responsible for the increased radiation, resulting from the interaction of these igneous rocks with the surrounding environment, warrant further investigation. It is hypothesized that the ^{226}Ra contained in these rocks (in the range of $75\text{--}288\text{ Bq}\cdot\text{kg}^{-1}$ [48]) significantly contributes to the observed higher radiation dose. These findings enrich our understanding of the natural gamma dose rate anomalies within the region and underline the geological underpinnings of localized heightened radiation levels.

Additionally, there is a gradient value outside the central region in Figure 5, which may be attributed to the specific materials used in the Parco Divisione Acque zone, the industrial zone Via Guido Maggiora, and the vicinity of the industrial zone Via del Lavoro. Observations suggest that the material composition in these zones differs from the adjacent zones. This corroborates the idea that one of the primary contributors to the radiation levels in the historic center is the presence of igneous rock. Furthermore, the sky blue zone lacks roads and, consequently, dwellings, leading to a scarcity of pavement. However, if there is pavement (as seen in Figure 5), it is mostly asphalt concrete, as reported in [47]. This indicates a decrease in a natural gamma dose rates.

In general, areas without roads and, consequently, fewer constructions or less pavement exhibit a reduced contribution to the natural gamma dose rate. This strongly supports the assertion that, in the Province of Asti, the elevation of the natural gamma dose rate is dependent on the materials used in the pavement and nearby buildings or installations.

Another crucial aspect to consider is the radio-geo-lithological analysis, specifically focusing on the concentrations of ^{222}Rn and ^{238}U , according to [49]. Given the prior establishment of the CE's significance within survey 1, it was compared with the new parameters, as shown in Table 3.

Table 3. Comparison of survey 1 with radio-geo-lithological analysis.

	Natural Gamma Dose Rate [$\mu\text{Sv}\cdot\text{h}^{-1}$] Median	Radio-Geo-Lithological Unit *	^{222}Rn [$\text{Bq}\cdot\text{m}^{-3}$] Median [49]	^{238}U [$\text{Bq}\cdot\text{kg}^{-1}$] Median [49]
CE	0.2161	Upper Tanaro, Stura di Demonte, Grana-Maira, Varaita, upper Po, Pellice-Chisone, and Chisola fluvial deposits; Upper Pleistocene–present	116	28
NE	0.1093	Marine, transitional, and continental deposits; Pliocene	72	47
NW	0.1068	Marine, transitional, and continental deposits; Pliocene	72	47
SE	0.1054	Rivoli-Avigliana morainic amphitheater glacial deposits; Pleistocene–Holocene	85	27
SW	0.1080	Marine, transitional, and continental deposits; Pliocene	72	47

* Most abundant and representative

Using the values from Table 3, the Pearson correlation coefficients and their associated p -values were obtained. The gamma dose rate versus the ^{222}Rn concentration exhibits a correlation coefficient of 0.948 with a p -value of 0.014, signifying a strong positive correlation with a statistical significance, while the gamma dose rate versus the ^{238}U concentration shows a correlation coefficient of -0.567 with a p -value of 0.319, indicating a moderate inverse linear correlation with no statistical significance. These findings suggest that, beyond the building materials used in the pavement, geology also plays a role and contributes, particularly in relation to the ^{222}Rn concentration affecting the natural gamma dose rate levels in the historic center of Asti.

4. Conclusions

An in situ radiometric survey and mapping of the Province of Asti has been successfully conducted.

The study findings confirm that natural radiation exposure varies based on location, ^{222}Rn concentration, and, especially, for the materials used in the construction of the city. In the Asti region, the average annual effective dose from the natural gamma dose rate is approximately 2.4 mSv per year, with relatively small interval values.

A cartographic representation of the work conducted has been produced, and the respective files will be made available to the TAS officer of the Command and the provincial NBCR coordinator. Upon material inspection, these resources will be accessible in the operational room. This study underscores that long-term exposure to natural sources of radiation falls within the world average concerning the associated health risks.

Natural radioactivity is a fundamental aspect of the environment, contributing significantly (80%) to the radiation dose received by the population (referred to as the 'natural

background’). The remaining exposure sources are attributed to medical diagnostics, the use of artificial radioactive substances, and industrial activities.

The most significant conclusion drawn from this study is that it serves as a baseline for understanding the natural gamma dose rate levels in the area. This baseline provides crucial insights for assessing and monitoring any future fluctuations or changes in radiation levels, thereby aiding in the formulation of effective strategies for radiation protection and risk management.

Author Contributions: Conceptualization, O.D.M., B.P. and L.S.-B.; methodology, O.D.M.; software, B.P.; validation, B.P., L.S.-B. and O.D.M.; formal analysis, B.P., L.S.-B. and O.D.M.; investigation, B.P., L.S.-B., and O.D.M.; resources, B.P., L.S.-B. and O.D.M.; data curation, B.P.; writing—original draft preparation, B.P., L.S.-B. and O.D.M.; writing—review and editing, B.P., L.S.-B., O.D.M. and D.P.F.; visualization, B.P., L.S.-B. and O.D.M.; supervision, B.P., L.S.-B., O.D.M., D.P.F. and A.P.; project administration, O.D.M.; funding acquisition, O.D.M. All authors have read and agreed to the published version of the manuscript.

Funding: This research received no external funding.

Institutional Review Board Statement: Not applicable.

Informed Consent Statement: Not applicable.

Data Availability Statement: Data are contained within the article.

Acknowledgments: The authors are indebted to the staff of the National Fire Brigade of the Provincial Command of Asti, for their unwavering support and help, without which this study could not have been carried out, and thanks also to the Atomic Defense Laboratory (Central Emergency Directorate) for their technical support.

Conflicts of Interest: The authors declare no conflicts of interest. The funders had no role in the design of the study; in the collection, analyses, or interpretation of the data; in the writing of the manuscript; nor in the decision to publish the results.

Abbreviations

The following abbreviations are used in this manuscript:

NBCR	Nuclear, Biological, Chemical, and Radiological
TAS	Topography Applied to Rescue
UCL	Local Command Unit
VVF	Vigili del Fuoco (Firefighters)

References

1. Rühm, W.; Azizova, T.; Bouffler, S.; Cullings, H.M.; Grosche, B.; Little, M.P.; Shore, R.S.; Walsh, L.; Woloschak, G.E. Typical doses and dose rates in studies pertinent to radiation risk inference at low doses and low dose rates. *J. Radiat. Res.* **2018**, *59*, ii1–ii10. [[CrossRef](#)]
2. Shankamma, K.; Nagaraja, K.; Sathish, L.A.; Kumar, K.C. A review on natural gamma radiation dose levels and its health effects. *Int. J. Health Allied Sci.* **2022**, *11*, 1. [[CrossRef](#)]
3. Egidi, P. *Introduction to Naturally Occurring Radioactive Material*; Technical Report; Oak Ridge National Lab.: Grand Junction, CO, USA, 1997.
4. Al-khawlany, A.H.; Khan, A.; Pathan, J.; Fatema, I. Assessment of potential radiological risks due to natural gamma radiations in some selected rock samples using y-ray spectrometry. *J. Phys. Conf. Ser.* **2020**, *1644*, 012004. [[CrossRef](#)]
5. Alwaeli, M.; Mannheim, V. Investigation into the current state of nuclear energy and nuclear waste management—A state-of-the-art review. *Energies* **2022**, *15*, 4275. [[CrossRef](#)]
6. Johansson, T.B.; Steen, P. *Radioactive Waste from Nuclear Power Plants*; Univ of California Press: Berkeley, CA, USA, 2022.
7. Khan, H.A.A.; Alshukri, A.S. Evaluation of environmental and health risks related with the management of medical waste in al najaf city. *J. Eng. Sci. Technol.* **2020**, *15*, 4383–4391.
8. Menon, S.; Kumar, L.S.V. Weaponizing radioactive medical waste-The looming threat. *Int. J. Nucl. Secur.* **2019**, *5*, 4. [[CrossRef](#)]
9. Sahoo, P.; Joseph, J. Radioactive hazards in utilization of industrial by-products: Comprehensive review. *J. Hazard. Toxic Radioact. Waste* **2021**, *25*, 03121001. [[CrossRef](#)]
10. Kant, K.; Gupta, R.; Kumari, R.; Gupta, N.; Garg, M. Natural radioactivity in Indian vegetation samples. *Int. J. Radiat. Res.* **2015**, *13*, 143–150.

11. Kovler, K.; Friedmann, H.; Michalik, B.; Schroeyers, W.; Tsapalov, A.; Antropov, S.; Bituh, T.; Nicolaidis, D. Basic aspects of natural radioactivity. In *Naturally Occurring Radioactive Materials in Construction*; Elsevier: Amsterdam, The Netherlands, 2017; pp. 13–36. [[CrossRef](#)]
12. Lolila, F.; Mazunga, M.S. Measurements of natural radioactivity and evaluation of radiation hazard indices in soils around the Manyoni uranium deposit in Tanzania. *J. Radiat. Res. Appl. Sci.* **2023**, *16*, 100524. [[CrossRef](#)]
13. René, M.; Akitsu, T. Nature, sources, resources, and production of thorium. In *Descriptive Inorganic Chemistry Researches of Metal Compounds*; IntechOpen: London, UK, 2017; pp. 201–212. [[CrossRef](#)]
14. Abbasi, A.; Kurnaz, A.; Turhan, Ş.; Mirekhtiary, F. Radiation hazards and natural radioactivity levels in surface soil samples from dwelling areas of North Cyprus. *J. Radioanal. Nucl. Chem.* **2020**, *324*, 203–210. [[CrossRef](#)]
15. Malikova, I.; Strakhovenko, V.; Ustinov, M. Uranium and thorium contents in soils and bottom sediments of lake Bolshoye Yarovoye, western Siberia. *J. Environ. Radioact.* **2020**, *211*, 106048. [[CrossRef](#)]
16. Missimer, T.M.; Teaf, C.; Maliva, R.G.; Danley-Thomson, A.; Covert, D.; Hegy, M. Natural radiation in the rocks, soils, and groundwater of Southern Florida with a discussion on potential health impacts. *Int. J. Environ. Res. Public Health* **2019**, *16*, 1793. [[CrossRef](#)]
17. Patel, K.S.; Sharma, S.; Maity, J.P.; Martín-Ramos, P.; Fiket, Ž.; Bhattacharya, P.; Zhu, Y. Occurrence of uranium, thorium and rare earth elements in the environment: A review. *Front. Environ. Sci.* **2023**, *10*, 1058053. [[CrossRef](#)]
18. Zanin, Y.N.; Zamirailova, A.; Eder, V. Uranium, thorium, and potassium in black shales of the Bazhenov Formation of the West Siberian marine basin. *Lithol. Miner. Resour.* **2016**, *51*, 74–85. [[CrossRef](#)]
19. Al-Khawlan, A.H.; Khan, A.; Pathan, J. Review on studies in natural background radiation. *Radiat. Prot. Environ.* **2018**, *41*, 215–222. [[CrossRef](#)]
20. United Nations Scientific Committee on the Effects of Atomic Radiation (UNSCEAR). *Sources and Effects of Ionizing Radiation*; Report to the General Assembly, with Scientific Annexes; United Nations: Vienna, Austria, 2020; E.00.IX.3; pp. 1–654.
21. Till, J.E.; Grogan, H.A. *Radiological Risk Assessment and Environmental Analysis*; Oxford University Press: Oxford, UK, 2008. [[CrossRef](#)]
22. Tye, A.; Milodowski, A.; Smedley, P. *Distribution of Natural Radioactivity in the Environment*; British Geological Survey: Nottingham, UK, 2017.
23. Marques, L.; Vale, A.; Vaz, P. State-of-the-art mobile radiation detection systems for different scenarios. *Sensors* **2021**, *21*, 1051. [[CrossRef](#)]
24. Musa, I.S.M. Environmental radiation: Natural radioactivity monitoring. In *Ionizing and Non-Ionizing Radiation*; IntechOpen: London, UK, 2019. [[CrossRef](#)]
25. Otori, Y.; Tokonami, S.; Sahoo, S.K.; Ishikawa, T.; Sorimachi, A.; Hosoda, M.; Kudo, H.; Pornnumpa, C.; Nair, R.R.K.; Jayalekshmi, P.A.; et al. Radiation dose due to radon and thoron progeny inhalation in high-level natural radiation areas of Kerala, India. *J. Radiol. Prot.* **2016**, *37*, 111. [[CrossRef](#)]
26. Delacroix, D.; Guerre, J.P.; Leblanc, P.; Hickman, C. Radionuclide and radiation protection data handbook 2002. *Radiat. Prot. Dosim.* **2002**, *98*, 1–168. [[CrossRef](#)]
27. Martin, J.E. *Physics for Radiation Protection: A Handbook*; John Wiley & Sons: Hoboken, NJ, USA, 2006. [[CrossRef](#)]
28. Shapiro, J. *Radiation Protection: A Guide for Scientists, Regulators, and Physicians*; La Editorial UPR: San Juan, Puerto Rico, 2002. [[CrossRef](#)]
29. Bossew, P.; Cinelli, G.; Hernández-Ceballos, M.; Cernohlawek, N.; Gruber, V.; Dehandschutter, B.; Menneson, F.; Bleher, M.; Stöhlker, U.; Hellmann, I.; et al. Estimating the terrestrial gamma dose rate by decomposition of the ambient dose equivalent rate. *J. Environ. Radioact.* **2017**, *166*, 296–308. [[CrossRef](#)]
30. Veiga, R.; Sanches, N.; Anjos, R.; Macario, K.; Bastos, J.; Iguatemy, M.; Aguiar, J.G.; Santos, A.; Mosquera, B.; Carvalho, C.; et al. Measurement of natural radioactivity in Brazilian beach sands. *Radiat. Meas.* **2006**, *41*, 189–196. [[CrossRef](#)]
31. Kotb, N.; Abd El Ghany, M.; El-Sayed, A.A. Radiological assessment of different monazite grades after mechanical separation from black sand. *Sci. Rep.* **2023**, *13*, 15389. [[CrossRef](#)]
32. Mishra, M.K.; Jha, S.; Patra, A.C.; Mishra, D.; Sahoo, S.; Sahu, S.; Verma, G.P.; Saindane, S.S.; Mitra, P.; Garg, S.; et al. Generation of map on natural environmental background absorbed dose rate in India. *J. Environ. Radioact.* **2023**, *262*, 107146. [[CrossRef](#)]
33. Veerasamy, N.; Murugan, R.; Kasar, S.; Inoue, K.; Kavasi, N.; Balakrishnan, S.; Arae, H.; Fukushi, M.; Sahoo, S. Geochemical characterization of monazite sands based on rare earth elements, thorium and uranium from a natural high background radiation area in Tamil Nadu, India. *J. Environ. Radioact.* **2021**, *232*, 106565. [[CrossRef](#)]
34. Tari, M.; Zarandi, S.A.M.; Mohammadi, K.; Zare, M.R. The measurement of gamma-emitting radionuclides in beach sand cores of coastal regions of Ramsar, Iran using HPGe detectors. *Mar. Pollut. Bull.* **2013**, *74*, 425–434. [[CrossRef](#)]
35. Shuaibu, H.K.; Khandaker, M.U.; Alrefae, T.; Bradley, D. Assessment of natural radioactivity and gamma-ray dose in monazite rich black Sand Beach of Penang Island, Malaysia. *Mar. Pollut. Bull.* **2017**, *119*, 423–428. [[CrossRef](#)]
36. Yasmin, S.; Barua, B.S.; Khandaker, M.U.; Kamal, M.; Rashid, M.A.; Sani, S.A.; Ahmed, H.; Nikouravan, B.; Bradley, D.A. The presence of radioactive materials in soil, sand and sediment samples of Potenga sea beach area, Chittagong, Bangladesh: Geological characteristics and environmental implication. *Results Phys.* **2018**, *8*, 1268–1274. [[CrossRef](#)]

37. Huang, Y.; Wen, W.; Liu, J.; Liang, X.; Yuan, W.; Ouyang, Q.; Liu, S.; Gok, C.; Wang, J.; Song, G. Preliminary Screening of Soils Natural Radioactivity and Metal (loid) Content in a Decommissioned Rare Earth Elements Processing Plant, Guangdong, China. *Int. J. Environ. Res. Public Health* **2022**, *19*, 14566. [CrossRef]
38. Rani, A.; Mittal, S.; Mehra, R.; Ramola, R. Assessment of natural radionuclides in the soil samples from Marwar region of Rajasthan, India. *Appl. Radiat. Isot.* **2015**, *101*, 122–126. [CrossRef]
39. Murthuza, K.M.; Surumbarkuzhali, N.; Thirukumaran, V.; Gandhi, M.S.; Ravi, A.; Ganesh, D.; Ravisankar, R. Statistical analysis of natural radioactivity measurements for the soil of Tiruvannamalai District, Tamilnadu, India. *Mater. Today Proc.* **2022**, *65*, 2606–2614. [CrossRef]
40. Ahmed, N.K. Measurement of natural radioactivity in building materials in Qena city, Upper Egypt. *J. Environ. Radioact.* **2005**, *83*, 91–99. [CrossRef]
41. Kumar, A.; Kumar, M.; Singh, B.; Singh, S. Natural activities of ²³⁸U, ²³²Th and ⁴⁰K in some Indian building materials. *Radiat. Meas.* **2003**, *36*, 465–469. [CrossRef]
42. Kocsis, E.; Tóth-Bodrogi, E.; Peka, A.; Adelikhah, M.; Kovács, T. Radiological impact assessment of different building material additives. *J. Radioanal. Nucl. Chem.* **2021**, *330*, 1517–1526. [CrossRef]
43. Sabbarese, C.; Ambrosino, F.; D’Onofrio, A.; Roca, V. Radiological characterization of natural building materials from the Campania region (Southern Italy). *Constr. Build. Mater.* **2021**, *268*, 121087. [CrossRef]
44. Amaral, E.; Amundsen, I.; Barišić, D.; Booth, P.; Clark, D.; Ditmars, J.; Dlouhy, Z.; Drury, N.; Gehrche, K.; Gnugnoli, G. *Characterization of Radioactively Contaminated Sites for Remediation Purposes*; IAEA-Tecdoc-1017; International Atomic Energy Agency: Vienna, Austria, 1998.
45. International Commission on Radiation Units and Measurements. *Determination of Dose Equivalents Resulting from External Radiation Sources*; ICRU: Ottawa, ON, Canada, 1985.
46. United Nations Scientific Committee on the Effects of Atomic Radiation and others. *Summary of Low-dose Radiation Effects on Health*; United Nations: New York, NY, USA, 2010.
47. Provincia di Asti. VIA-Progetti e Lavori in Corso. 2023. Available online: <https://www.provincia.asti.it/it/page/progetti-e-lavori> (accessed on 13 November 2023).
48. Najam, L.; AL-Jomaily, F.; AL-Farha, E. Natural radioactivity levels of limestone rocks in northern Iraq using gamma spectroscopy and nuclear track detector. *J. Radioanal. Nucl. Chem.* **2011**, *289*, 709–715. [CrossRef]
49. Chiaberto, E.; Falletti, P.; Magnoni, M. Radon mapping in Piedmont (North-West Italy): A radio-geo-lithological approach. *J. Eur. Radon Assoc.* **2022**, *3*, 7719. [CrossRef]

Disclaimer/Publisher’s Note: The statements, opinions and data contained in all publications are solely those of the individual author(s) and contributor(s) and not of MDPI and/or the editor(s). MDPI and/or the editor(s) disclaim responsibility for any injury to people or property resulting from any ideas, methods, instructions or products referred to in the content.